ChemPubSoc Europe

DOI: 10.1002/cctc.201500097

CHEMCATCHEM Full Papers

Robust and Recyclable Nonprecious Bimetallic Nanoparticles on Carbon Nanotubes for the Hydrogenation and Hydrogenolysis of 5-Hydroxymethylfurfural

Lili Yu, Le He, Jin Chen, Jianwei Zheng, Linmin Ye,* Haiqiang Lin, and Youzhu Yuan*[a]

Selective hydrogenation and hydrogenolysis of 5-hydroxymethylfurfural were performed with carbon nanotube-supported bimetallic Ni–Fe (Ni–Fe/CNT) catalysts. The combination of Ni and Fe in an appropriate atomic ratio of Ni/Fe (2.0) significantly increased the selectivity to 2,5-furandimethanol or 2,5-dimethylfuran depending on the reaction temperature. The selectivities to 2,5-furandimethanol and 2,5-dimethylfuran were as high as 96.1% at 383 K and 91.3% at 473 K, respectively. The characterization results confirmed that bimetallic particles with sizes less than 7 nm were formed on the catalyst. Several key molecules related to 5-hydroxymethylfurfural transformation were used to investigate the product distribution and reaction pathway. The results indicated that the formation of Ni–Fe alloy species is beneficial to the selective cleavage of the C–O bond. Recycling experiments showed that the catalyst can be easily separated with a magnet and reused several times without significant loss of activity.

Introduction

Because of diminishing fossil fuels, people are searching for new ways to efficiently use sustainable energy source. The widespread, abundant, inexpensive, and renewable biomass resource has aroused much interest in both scientific and industrial communities because of its potential use in producing fuels and chemicals.[1] 5-Hydroxymethylfurfural (HMF) has been identified as one of the top 10 bio-based platform molecules with significant market potential.[2] HMF can be either oxidized to furan 2,5-dicarboxylic acid[3] or hydrogenated to 2,5-furandimethanol (FDM)[4] under mild conditions, both of which are useful building blocks in polymer industry. However, the hydrogenolysis of HMF to 2,5-dimethylfuran (DMF) is attractive[1,5] because DMF is a better liquid fuel than gasoline owing to its higher energy content, boiling point, and octane number. The hydrogenation of HMF results in a mixture of side chain- and ring-hydrogenated products along with ring-opening products. The key challenge in upgrading HMF is improving the product selectivity. DMF is obtained through hydrogenation or transfer hydrogenation reactions with molecular hydrogen,[5,6] formic acid,[7] alcohol,[8] and even water[9] as hydrogen donors. In general, a noble metal catalyst is the first choice for the hydrogenation reaction. The monometallic Ru/C presented 60.3% yield of DMF in *n*-butanol. However, the yield of DMF increased to 94.7% if THF is used as a solvent.[10] Similarly, the Pd/C catalyst gives poor selectivity to DMF in the ionic liquid 1-ethyl-3-methylimidazolium chloride but 100% yield in supercritical CO_2 and H_2O used as reaction media.[11] These findings suggested that an appropriate solvent may benefit the selectivity. In addition, the additives in the reaction system can affect the selectivity to the product. In the Pd/C system, the decarbonylation reaction occurs easily, forming furfuryl alcohol as the major product without an additive. The decarbonylation reaction is suppressed in the presence of formic acid, which leads to a high selectivity to DMF.[12] Moreover, adding second metal to form an alloy, such as Cu–Ru[13] or Pd–Au,[14] promotes the selective hydrogenation of HMF to DMF. Wang et al.[15] developed a method for producing the Pt–Co alloy in a hollow carbon nanosphere, and the catalyst is found to be suitable for the hydrogenation of HMF, with a yield of DMF up to 98%, which substantially exceeds the best results reported in the literature.

However, developing nonprecious metal catalyst systems as an alternative to precious metal catalyst systems is favorable for both economic and engineering aspects. Given the wide application of the Ni-based catalyst in hydrogenation reactions, Raney-type metals (Cu, Co, and Ni) have been used to investigate this reaction. The Raney Ni catalyst achieved 88.5 and 96% yields of DMF and 2,5-dihydroxymethyltetrahydrofuran, respectively. The authors pointed out that the high temperature promoted the deoxygenation step.[16] Notably, the ring hydrogenation product was obtained at a low temperature with the Raney Ni catalyst owing to its excellent hydrogenation abil-

[a] L. Yu, L. He, J. Chen, J. Zheng, Dr. L. Ye, Dr. H. Lin, Prof. Dr. Y. Yuan
State Key Laboratory of Physical Chemistry of Solid Surfaces and
National Engineering Laboratory for Green Chemical
Production of Alcohols-Ethers-Esters
Collaborative Innovation Center of Chemistry for Energy Materials
College of Chemistry and Chemical Engineering
Xiamen University, Xiamen 361005 (P.R. China)
Fax: (+86) 592-2183047
E-mail: lmye@xmu.edu.cn
yzyuan@xmu.edu.cn

Supporting Information for this article is available on the WWW under http://dx.doi.org/10.1002/cctc.201500097.

ity. Huang et al.[17] proposed a Ni–W_2C/C system in which Ni showed hydrogenation ability and W_2C offered deoxygenating ability. Synergism of these species achieved the best result for the conversion of HMF to DMF, with yield up to 96%. Kumalaputri et al.[18] found that Cu-doped porous metal oxides can effectively convert HMF to FDM in 97% yield at 373 K. Meanwhile, Ru-promoted Cu-doped porous metal oxides convert HMF to DMF in 61% yield at 493 K. Compared with the Ni-based catalyst, the weaker hydrogenolysis ability of the Cu-based catalyst may reflect the low selectivity to DMF.

Herein, Ni–Fe/CNT catalysts with different Ni/Fe atomic ratios were synthesized by using the wet impregnation method. The catalysts were evaluated under different reaction conditions to investigate the product distribution. The catalyst showed tunable selectivity FDM or DMF for the hydrogenation of HMF, depending on the reaction temperature. Moreover, the product distribution was investigated by using different intermediates as substrates to understand the reaction pathway. The results of this study provide not only a new catalytic system for producing DMF and FDM from HMF but also an understanding of the structural and catalytic properties of bimetallic Ni–Fe/CNT catalysts.

Results and Discussion

Characterization results

The chemical compositions and textural properties of all catalysts are summarized in Table 1. The bimetallic Ni–Fe catalysts were prepared by keeping the Ni loading constant at 10% but varying Ni/Fe atomic ratios. The Ni loadings and Ni/Fe ratios are close to their theoretical values, as determined from X-ray fluorescence spectroscopy analysis. The BET surface areas of Ni–Fe/CNT catalysts ranging from 132 to 140 $m^2 g^{-1}$ are insignificantly lower than those of pure CNT carriers (168 $m^2 g^{-1}$), which indicates that the Ni–Fe nanoparticles were deposited on CNTs without causing the collapse of the nanostructure. Meanwhile, the slightly decreasing pore volume and pore diameter indicated that most of the Ni–Fe nanoparticles were on the surface instead of inside the CNTs.

Compared with Ni/CNTs, the average particle size of Ni–Fe/CNTs decreased from 7.4 to 6.5 nm. Therefore, introducing Fe species promoted the dispersion of Ni. However, the metal dispersion decreased to 15.4% if the Ni/Fe ratio was set to 1. The excess of Fe species in the form of Fe_3O_4 may block the active site of Ni, which causes the decrease in adsorption ability.

The temperature-programmed reduction of hydrogen (H_2-TPR) profiles of the as-calcined Ni–Fe/CNT catalysts with different Ni/Fe atomic ratios are shown in Figure 1. In the literature, the peak at approximately 680 K is attributed to the reduction of Fe^{3+} to Fe^{2+} in the oxides, and the peak at 880 K is assigned to the reduction of Fe^{2+} to Fe.[19] However, these two peaks were likely overlapped, probably owing to the well dispersion of Fe species on the CNT surface (Figure 1 f), which implied that Fe species of the Fe/CNT catalyst were difficult to be reduced under present conditions for the catalyst preparation (under 5% H_2/95% N_2 at 673 K for 4 h). The reduction profile for the monometallic Ni/CNT catalyst displayed a broad peak ranging from 673 to 923 K with the maximum at 800 K, which is typically attributed to the reduction of NiO to Ni. Adding Fe species slightly shifted the reduction peak to lower temperature, which indicated the occurrence of the interaction between Ni and Fe species. In addition, a shoulder peak appeared at approximately 900 K if the Ni/Fe ratio was set higher than 1, which suggested the reduction of isolated iron oxides. An excessive addition of Fe species leads to a new peak observed at 920 K (Figure 1 e).

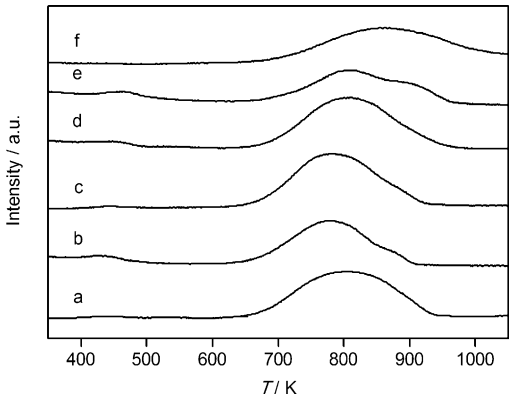

Figure 1. H_2-TPR profiles of Ni–Fe/CNT catalysts with different Ni/Fe atomic ratios: a) Ni/CNTs; b) Ni_{10}–Fe_1/CNTs; c) Ni_5–Fe_1/CNTs; d) Ni_2–Fe_1/CNTs; e) Ni_1–Fe_1/CNTs; f) Fe/CNTs.

Table 1. Physicochemical properties of Ni–Fe/CNT catalysts.

Sample	M[a] [wt%]	S_{BET} [$m^2 g^{-1}$]	V_{pore}[b] [$cm^3 g^{-1}$]	D_{pore} [nm]	$D_{particle}$[c] [nm]	D_{Ni}[d] [%]
CNTs	–	168	0.22	6.0	–	–
Ni/CNTs	10.3	134	0.18	5.9	7.4	18.3
Ni_{10}–Fe_1/CNTs	9.9 (11.0)	134	0.17	5.6	6.5	17.6
Ni_5–Fe_1/CNTs	9.8 (5.5)	136	0.15	5.6	6.5	17.1
Ni_2–Fe_1/CNTs	9.6 (2.1)	138	0.16	5.6	6.7	16.2
Ni_1–Fe_1/CNTs	9.2 (1.1)	140	0.16	5.3	6.8	15.4
Fe/CNTs	4.8	132	0.18	5.8	–	–

[a] Determined from X-ray fluorescence spectroscopy analysis; the data in parentheses represent the Ni/Fe atomic ratio; [b] Obtained at $P/P_0 = 0.99$; [c] $D_{particle}$ = average particle size, based on TEM data; [d] Calculated by CO chemisorption.

The XRD patterns of the as-reduced catalysts with different Ni/Fe atomic ratios are shown in Figure 2. The diffraction lines of Ni (111), (200), (220) and Fe (110), (200), (211) for the monometallic samples were observed at $2\theta = 44.4$, 51.7, 76.1° and $2\theta =$ 44.6, 64.7, 82.3°, respectively (JCPDS nos. 00-001-1258 and 00-001-1262). No significant diffraction lines of Fe species were observed (Figure 2 g). The

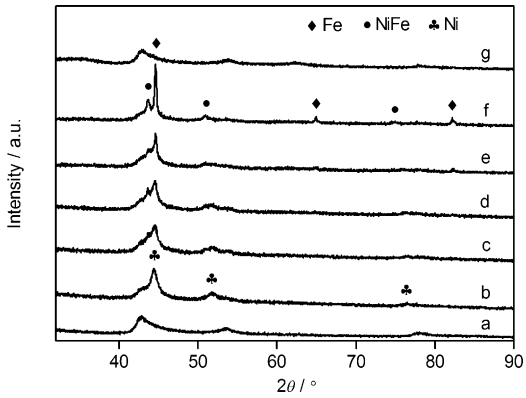

Figure 2. XRD patterns of the as-reduced Ni–Fe/CNT catalysts with different Ni/Fe atomic ratios: a) CNTs; b) Ni/CNTs; c) Ni_{10}–Fe_1/CNTs; d) Ni_5–Fe_1/CNTs; e) Ni_2–Fe_1/CNTs; f) Ni_1–Fe_1/CNTs; g) Fe/CNTs.

results suggested that Fe species were well dispersed on CNTs. The lines appeared at $2\theta = 43.5$, 50.8, 74.8° with the introduction of Fe species into Ni/CNTs, which indicated the formation of the Ni–Fe alloy (JCPDS no. 00-023-0297) (Figure 2c–f). In this case, the Ni/Fe ratios ranged from 1 to 5. The diffraction lines of Fe was clearly observed at $2\theta = 64.7$ and 82.3° in the XRD patterns of the as-reduced Ni–Fe/CNT sample with Ni/Fe = 1 (Figure 2f). These findings are consistent with the H_2-TPR results.

The TEM images and particle size dispersions of the as-reduced catalysts are shown in Figure S1. The average particle size of monometallic Ni/CNTs was 7.4 nm. With the addition of Fe species, the particle size of bimetallic Ni–Fe/CNT catalysts decreased slightly and maintained at approximately 6.5 nm. These findings indicate that adding Fe species is beneficial to disperse Ni. The scanning transmission electron microscope-energy dispersive X-ray analysis (STEM-EDX) elemental mappings and the linear scanning pattern of the Ni_2–Fe_1/CNT catalyst are shown in Figure 3. The STEM-EDX elemental mappings were adopted to investigate the distribution of Ni and Fe atoms. The Fe atoms dissolved homogeneously into the Ni clusters as indicated by the complete overlapping of Ni and Fe signals. The linear scanning result in Figure 3e also confirmed the STEM-EDX elemental mapping result. The Ni–Fe structure was further characterized by high-resolution TEM (Figure 3f). Well-resolved lattice fringes were clearly observed, and two types of lattice fringes with interplanar spacings of 0.2078 and 0.1796 nm appeared, which are ascribed to the (111) and (200) planes, respectively. The angle between the planes was 55.2°. The results were approximate to the theoretical values for the Ni–Fe alloy nanocrystal (JCPDS no. 00-023-0297). Thus, the Ni–Fe alloy was formed and well-dispersed on the surface of CNTs with an appropriate Ni/Fe ratio.

The X-ray photoelectron spectroscopic (XPS) data provide further evidence for the formation of Ni–Fe alloys. The Fe 2p and Ni 2p XPS data of the as-reduced Fe/CNTs and Ni_2–Fe_1/CNTs are depicted in Figure S3. Although the samples were transferred to the XPS chamber under N_2 atmosphere without bringing it into contact with air, the partial oxidation of reduced entities could not be completely excluded. According to the published data[20] and an online database (http://srdata.nist.gov/XPS), three kinds of Ni could be identified, as shown in Figure S3c: Ni ($2p_{3/2}$: 853.1 eV and $2p_{1/2}$: 870.8 eV), NiO (855.4 and 873.1 eV), and $Ni(OH)_2$ (861.2 and 880.0 eV). The peak at approximately 711 eV is attributed to Fe^{3+} $2p_{3/2}$, which demonstrates the presence of iron oxide. Iron oxide species on Fe/CNTs were nearly intact after reduction under present conditions. However, a new peak appears at 707.2 eV in the Ni_2–Fe_1/CNT catalyst, which is assigned to Fe species.[21] This result confirms that partial Fe^{3+} species are reduced upon the addition of Ni. The finding supports the results obtained from XRD and TEM analyses that a portion of Fe species interacts with Ni by the formation of Ni–Fe alloys.

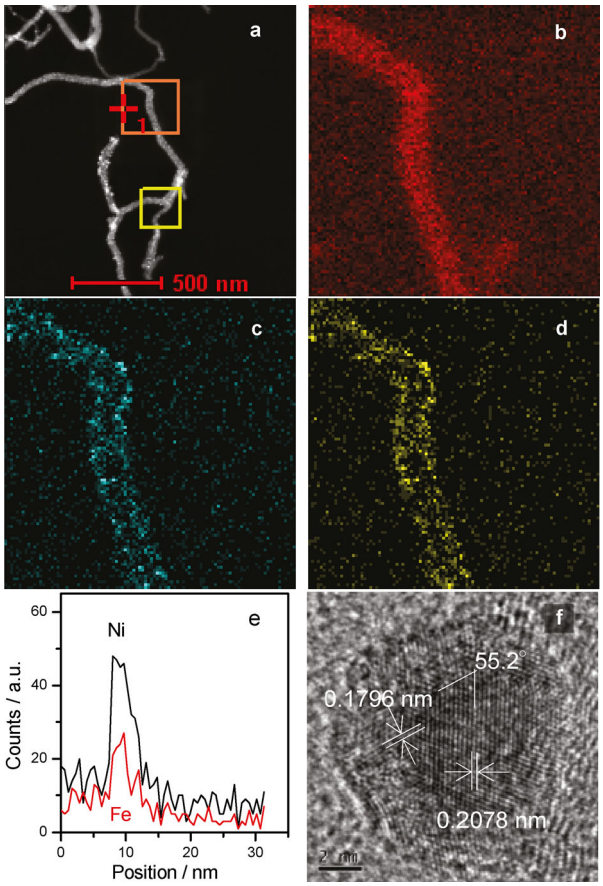

Figure 3. a) TEM dark-field image; b–d) STEM-EDX elemental mappings of C–K, Ni–K, and Fe–K; e) linear scanning pattern; and f) high-resolution TEM image of the Ni_2–Fe_1/CNT catalyst.

Hydrogenation and hydrogenolysis of HMF

The catalytic performance of Ni–Fe/CNTs at different reaction temperatures is summarized in Table 2. The Fe/CNT catalyst showed low catalytic activity at both low and high temperatures, which confirms that Fe species alone has poor effect on the hydrogenation of HMF. Meanwhile, the monometallic Ni/CNT catalyst shows high conversion but poor selectivity at 383 or 473 K. In addition, the byproducts of the reaction, including

Table 2. Catalytic performance of Ni–Fe/CNTs for the selective hydrogenation and hydrogenolysis of HMF.[a]

Catalyst	T [K]	Conversion [%]	Selectivity [%]				
			FDM	MFM	DMF	DMTHF	Others[b]
Ni/CNTs	383[c]	100	76.4	6.5	5.4	0.5	11.2
	473[d]	100	13.4	10.0	46.3	7.9	22.4
Ni_{10}–Fe_1/CNTs	383[c]	100	87.7	3.2	0.9	0	8.2
	473[d]	100	0	0	75.8	3.2	21.0
Ni_5–Fe_1/CNTs	383[c]	100	92.3	2.3	0.5	0	4.9
	473[d]	100	0	0	86.5	0	13.5
Ni_2–Fe_1/CNTs	383[c]	100	96.1	2.1	0	0	1.8
	473[d]	100	0	2.4	91.3	0	6.3
Ni_1–Fe_1/CNTs	383[c]	99.2	97.5	0	0	0	2.5
	473[d]	100	20.0	31.3	44.6	0	4.1
Fe/CNTs	383[c]	0	–	–	–	–	–
	473[d]	3.2	31.2	0	0	0	68.8
Ni/CNTs	383[c]	100	77.7	5.6	8.1	1.0	7.6
Fe/CNTs[e]	473[d]	100	16.3	8.5	54.9	6.8	13.5

[a] Reaction conditions: 0.050 g of the catalyst, 4.0 mmol of HMF, 20 mL of *n*-butanol, $P(H_2) = 3.0$ MPa; [b] Mainly containing ethers, decarbonylation product, ring-opening product, and humin; [c] $t = 18$ h; [d] $t = 3$ h; [e] Physical mixture of Ni/CNTs and Fe/CNTs.

decarbonylation product [5-methylfurfural (MF)], ring hydrogenation product [2,5-dimethyltetrahydrofuran(DMTHF)], ring-opening product [1,2-hexanediol (HD)], and etherification product, were detected. FDM is the major product at 383 K (Table 2). Therefore, the aldehyde group of HMF can be easily hydrogenated to the hydroxyl group with Ni/CNT and Ni–Fe/CNT catalysts. All catalysts except Fe/CNTs induced HMF conversion as high as 100% at 473 K. FDM was further hydrogenolyzed to yield 5-methyl-2-furanmethanol (MFM) and DMF. The selectivity to DMF showed a volcano-type behavior with increasing Fe loading. The Ni_2–Fe_1/CNT catalyst presented the highest selectivity to DMF (91.3%) than did the other catalysts. These results reveal that the formation of the Ni–Fe alloy is beneficial to the cleavage of the C–O bond, which yields DMF as the major product at 473 K. Sitthisa et al.[22] used DFT calculations to investigate geometries and relative stabilities of the possible furfural species adsorbed on the surface of pure Ni (111) and a bimetallic Ni–Fe (111) alloy. Fe species are beneficial to the adsorption of the furan ring owing to their oxophilic nature. Hence, a stronger interaction between furfural and Ni–Fe than that between furfural and pure Ni is expected. The results showed that the C–O bond on Ni–Fe (111) was longer than that on pure Ni (111), which indicated an easier cleavage of the C–O bond on Ni–Fe (111).[22]

To determine whether the interaction between Ni and Fe is the reason for high selectivity, a control experiment was conducted with a physical mixture of Ni/CNTs and Fe/CNTs as a catalyst. The conversion and product distribution were similar to those of pure Ni/CNTs. Therefore, the change in the product distribution of Ni–Fe/CNTs is mainly due to the formation of Ni–Fe alloys, which have been identified by XRD and TEM measurements. Furthermore, we calculated the turnover frequency, which is listed in Table S1. The decreasing turnover frequency from 93.2 to 28.7 h^{-1} with increasing Fe loading reveals that adding Fe inhibits the hydrogenation ability (from the aldehyde group to the hydroxyl group) of the Ni catalyst.

We also prepared bimetallic Ni–Fe catalysts on different supports with a fixed Ni/Fe ratio of 2 (Table S2). Ni_2–Fe_1/CNTs show higher conversion than Ni_2–Fe_1/AC (activated carbon), which can be due to the smaller metal particle size. In addition, contrary to Ni_2–Fe_1/CNTs, the XRD pattern in Figure S2 indicate that no peak attributed to the Ni–Fe alloy was identified in Ni_2–Fe_1/SiO_2 and Ni_2–Fe_1/Al_2O_3, which confirmed the promoting effect of the Ni–Fe alloy. The effect of different solvents was also investigated. In the literature,[10,13] *n*-butanol was selected as a good solvent for the present catalytic reaction. We evaluated the performance of Ni_2–Fe_1/CNTs by using different solvents such as methanol, ethanol, and *n*-propanol in addition to *n*-butanol. The results showed that the catalyst could present a superior performance only if *n*-butanol was used as the solvent (Table S3). The etherification between HMF and alcoholic solvents is a major reaction competing with hydrogenolysis. The alcohols with a shorter chain favor the etherification reaction owing to less steric effects.[23] In addition, dehydration is a key step in the hydrogenolysis of HMF to DMF. Therefore, solvent properties such as polarity could affect the interactions between the solvent and the reactant and between the solvent and the catalyst and thus affect the efficiency of HMF hydrogenolysis. The selectivity to DMF increased with the decrease in solvent polarity (from methanol to *n*-butanol), possibly owing to the decrease in interactions between the solvent and the reactant and between the solvent and the catalyst, which enhanced the interaction of HMF with the active sites of the catalyst.

The effect of reaction temperature was further examined from 393 to 493 K at 3.0 MPa with the Ni_2–Fe_1/CNT catalyst. The results presented in Figure 4 strongly suggest that the reaction temperature markedly affected the product distribution. FDM, the primary hydrogenation product, was the major product at a low temperature (393 K) with a selectivity of 96.4%. As

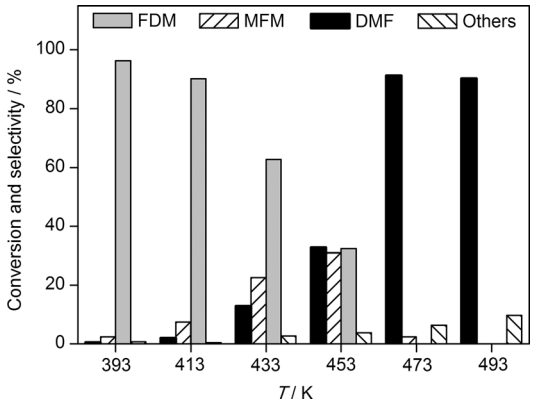

Figure 4. Catalytic performance of Ni_2–Fe_1/CNT catalysts under the following reaction conditions: 0.050 g of the catalyst, 4.0 mmol of HMF, 20 mL of *n*-butanol, $P(H_2) = 3.0$ MPa, $t = 3$ h.

the temperature increased, the selectivity to DMF, the hydrogenolysis product, increased quickly and reached 91.3% at 473 K. The selectivity to MFM was less than 31%, and it showed a volcano-type behavior with increasing temperature, which indicated that MFM was easily hydrogenolyzed to DMF.

Several intermediates were further studied with Ni_2–Fe_1/CNTs at 473 K for 3 h, which was the reaction condition most ideal for DMF formation (Table 3). The above-mentioned results

Table 3. Catalytic evolution of key molecules related to HMF transformation over Ni_2–Fe_1/CNTs.[a]

Substrate	Conversion [%]	Selectivity [%]				
		MFM	DMF	DMTHF	HD	Others[b]
FDM	100	2.9	80.4	0.4	0	16.3
FDM[c]	100	7.9	57.5	11.3	3.9	19.4
MFM	100	–	96.0	0.9	0	3.1
MFM[c]	100	–	72.7	13.2	4.5	9.6
MF	100	4.6	90.9	0.5	0	4.0
MF[c]	100	8.8	67.2	9.7	5.4	8.9
DMF	4.6	–	–	96.5	–	3.5
DMF[c]	35.7	–	–	95.3	–	4.7
DMTHF	0	0	0	0	0	0

[a] Reaction conditions: 0.050 g of the catalyst, 4.0 mmol of the substrate, 20 mL of *n*-butanol, $P(H_2)=3.0$ MPa, $T=473$ K, $t=3$ h; [b] Mainly containing ethers and humin; [c] Ni/CNTs as the catalyst.

indicate that FDM may be an important intermediate for the hydrogenation of HMF at low temperatures. Therefore, FDM was initially introduced as a substrate. Because FDM has two OH groups as compared with MFM and MF, ether compounds could be readily formed through the dehydration of two FDM molecules as well as FDM and an alcoholic solvent, with pure FDM as a substrate.[24] The total amount of ether products was approximately 10%. These side reactions lowered the selectivity to DMF. No HD was detected with FDM as a substrate, which implied that the ring-opening reaction did not occur with the bimetallic Ni–Fe catalyst. Similar phenomena were observed with MFM and MF as substrates. Meanwhile, an insignificant ring-opening product was observed when FDM, MFM, and MF were used as substrates. Less than 5% DMF converted to DMTHF with 96.5% selectivity, considering DMF is more stable than the partially reduced intermediate FDM or MFM. No conversion of DMTHF was observed, which confirmed the previous result. Furthermore, the product distribution was investigated by using Ni/CNTs. Contrary to the results obtained with Ni_2–Fe_1/CNTs, DMF was obtained at a moderate selectivity of 57.5–72.7% along with DMTHF and HD as byproducts. The different results obtained with DMF as a substrate and Ni_2–Fe_1/CNTs and Ni/CNTs catalysts reveal that the formation of the Ni–Fe alloy inhibits further hydrogenation of the furan ring, which minimizes the yield of DMTHF.

The possible reaction pathway for the conversion of HMF is illustrated in Scheme 1. The solid and dashed arrows refer to the reaction pathways catalyzed by Ni_2–Fe_1/CNTs and Ni/CNTs, respectively. With the Ni_2–Fe_1/CNT catalyst, HMF was initially

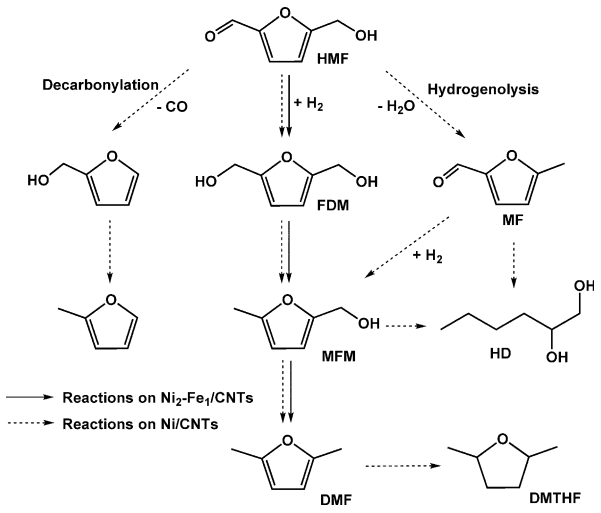

Scheme 1. Possible reaction pathway for the conversion of HMF.

hydrogenated to FDM and then further deoxygenated to form MFM and DMF. The final product DMF was stable under the given reaction conditions. By contrast, three reactions occurred, namely, hydrogenation, decarbonylation, and hydrogenolysis, with Ni/CNT catalysts. The decarbonylation product was obtained in a small amount (<2%). MF can either hydrogenate to MFM or form the ring-opening product HD, which is also derived from MFM. Notably, the furan ring can be saturated to form DMTHF because of the highly hydrogenation ability of the monometallic Ni/CNT catalyst.

Catalyst stability

The recycling results of Ni_2–Fe_1/CNTs are presented in Figure 5. The catalyst could easily be recovered with a magnet in a few minutes and then reused several times like Ce–Ni/Al_2O_3[25] (Figure S5). The conversion of HMF was maintained at 100% in the whole recycling experiment. However, the selectivity to DMF gradually decreased to 74.2% after the sixth run. The intermediates such as FDM and MFM were detected along with DMF. Specifically, the selectivity to DMF increased up to 85.4%

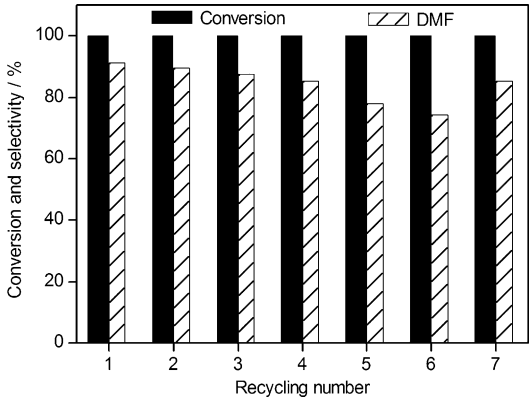

Figure 5. Recycling results of Ni_2–Fe_1/CNT catalysts under the following reaction conditions: 0.050 g of the catalyst, 4.0 mmol of the substrate, 20 mL of *n*-butanol, $P(H_2)=3.0$ MPa, $T=473$ K, $t=3$ h.

if the catalyst was recalcined at 573 K and reused for the seventh run.

The Ni content in the aqueous phase was checked after each cycle by using inductively coupled plasma atomic emission spectrometry. The results indicate that the amount of Ni and Fe species leached is lower than the detectable level (Table S4). The XRD patterns of the as-reduced Ni_2–Fe_1/CNTs and the used catalyst (Figure S6) demonstrate that the intensity of the metallic Ni diffraction peaks of the catalysts obtained after the reaction is only slightly higher than that of the peaks of the as-reduced catalysts. Therefore, the aggregation of Ni nanoparticles during the reaction is minimal. The TEM image gave an intuitive Ni particle size of 7.2 nm after the reaction, which was slightly larger than that of the fresh catalyst. The thermogravimetric profiles provide an important information on the reactivity (Figure S7). Compared to the fresh Ni_2–Fe_1/CNT catalyst, the sudden weight loss of the used catalyst from 600 to 800 K is mainly due to the combustion of the organic compound, for example, the small amount of humin derived from the polymerization of HMF. Therefore, deactivity may be due to the slow formation of the polymer, which covered the activity center of the catalyst.

Conclusions

We developed an inexpensive, effective, nonprecious carbon nanotube-supported bimetallic Ni–Fe (Ni–Fe/CNT) catalyst for the selective hydrogenation and hydrogenolysis of 5-hydroxymethylfurfural with molecular hydrogen as a hydrogen donor. The catalyst with an appropriate Ni/Fe atomic ratio showed an excellent selectivity to 2,5-furandimethanol or 2,5-dimethylfuran at 383 and 473 K, respectively. Contrary to the monometallic Ni/CNT catalyst, a negligible amount of the overhydrogenation product of the furan ring (2,5-dimethyltetrahydrofuran) was observed. The XRD and TEM results indicated that Ni–Fe alloy species were formed on the surface of CNTs. Detailed research shows that Ni–Fe alloy species are beneficial to the cleavage of the C–O bond at a higher reaction temperature. The catalyst can be easily separated with a magnet and reused several times. The high activity and stability of the Ni_2–Fe_1/CNT catalyst under the given reaction conditions suggest that the catalyst is feasible and a promising material for 2,5-dimethylfuran production through the selective hydrogenation and hydrogenolysis of 5-hydroxymethylfurfural.

Experimental Section

Catalyst preparation

All the reagents were used as received without further purification. CNTs (diameter = 10–20 nm) with a purity of 95% were purchased from Shenzhen Nanotech Port Co., Ltd. First, pristine CNTs were purified and functionalized in concd HNO_3 (68 wt%) at 353 K for 16 h and heated to reflux to remove amorphous carbon and the remaining catalyst residues. Then, the treated CNTs were filtered, extensively washed with deionized water until the pH of the rinsing water became neutral, and dried at 373 K overnight. Supported bimetallic Ni–Fe catalysts were prepared through coimpregnation with an aqueous solution containing two metal precursors, namely, $Ni(NO_3)_2{\cdot}6H_2O$ (98%, Alfa Aesar) and $Fe(NO_3)_3{\cdot}9H_2O$ (98%, Sigma–Aldrich). After impregnation and solvent removal by evaporation, the produced solids were dried overnight at 383 K. All the dried samples were calcined at 573 K in air for 4 h. Before the reaction, the samples were reduced by 5% H_2/95% N_2 at 673 K for 4 h. The bimetallic catalyst was labeled as Ni_x–Fe_y/CNTs, in which x and y were the atomic ratios of Ni and Fe, respectively.

Characterization

The N_2 adsorption–desorption isotherms were measured at 77.3 K with a Micromeritics TriStar II 3020 porosimetry analyzer. Before adsorption, the sample was degasified at 473 K for 2 h. The specific surface area was obtained by using the BET method at $P/P_0 = 0.05$–0.3. By using the Barret–Joyner–Halenda method, the average pore diameter and pore size distribution were evaluated from the pore size distribution curve, which was obtained by analyzing the desorption isotherm branch. The total pore volume of the samples depended on the amount of N_2 vapor adsorbed at $P/P_0 \approx 0.99$.

The Ni and Fe contents were determined with a Bruker S8 TIGER X-ray fluorescence spectrometer. The samples were prepared by mixing the catalyst (0.20 g) and boric acid (0.80 g) and compressing into tablets (diameter = 36 mm; thickness = 2 mm).

H_2-TPR was performed with a Micromeritics AutoChem II 2920 chemisorption analyzer. Samples (0.10 g) were weighed and flushed with high purity He (flow rate: 30 $cm^3 min^{-1}$) at 473 K for 1 h and then cooled to 323 K. Subsequently, 5% H_2/95% Ar was flowed through the samples while the temperature was increased from 323 to 1173 K (heating rate: 10 $K min^{-1}$). The thermal conductivity detector signal automatically recorded the H_2 consumption.

The XRD pattern was recorded with a Philips PANalytical X'pert PRO diffractometer equipped with a graphite monochromator and a CuK_α radiation source (40 kV and 30 mA), scanning at $2\theta = 20$ to 90°. The results were compared with the standard powder XRD data (in the JCPDS database).

Static CO chemisorption was measured with a Micromeritics ASAP 2020 (M + C) apparatus. The catalysts were treated by a flow of 5% H_2/95% N_2 with the increase in temperature from 303 to 673 K (heating rate: 2 $K min^{-1}$) and then cooled to RT. The as-prepared catalysts were then soaked in H_2 at 673 K for 15 min, evacuated for 60 min, and cooled to 308 K. After pretreatment, the catalysts were analyzed by pumping CO gas at 308 K. The initial isotherm was then measured. A 30 min evacuation at 308 K was then performed to remove the reversibly adsorbed H_2 on the catalyst surface before performing the measurement for a second isotherm under conditions similar to those of the first isotherm. The difference between the first and second isotherms reflected the quantity of irreversibly chemisorbed H_2 on the catalyst sample.

The TEM images were obtained with a Tecnai F20 electron microscope operated at an accelerating voltage of 200 kV. The powder was dispersed in ethanol by ultrasonication for 10 min, and then drops of suspensions were deposited on a copper grid coated with carbon. The statistical mean diameter of the nanoparticles was measured by counting at least 200 particles for each catalyst.

XPS was performed with a PHI Quantum 2000 Scanning ESCA Microprobe with an AlK_α radiation source ($h\nu = 1486.6$ eV). The binding energy was calibrated from that of C 1s (284.6 eV). The reduced samples were attached to the sample holder with conductive

double-sided adhesive tape and transferred to the XPS chamber immediately under N_2 atmosphere.

Inductively coupled plasma atomic emission spectrometry was performed with a Thermo Elemental IRIS Intrepid II XSP spectrometer. The filtrate (2.0 mL) was treated by aqua regia at 353 K for 30 min to decompose the organic compounds, and the resultant solution was heated up to 363 K to evaporate the solvent. The residue was diluted with 5% HNO_3 and filtered in a 25 mL volumetric flask before the measurement.

The thermogravimetric profiles were recorded on a NETZSCH STA 449C analyzer with Al_2O_3 as a reference. The measurements were performed with a dynamic temperature program of 298–1073 K (heating rate: 10 K min^{-1}) in air.

Catalytic testing

The catalytic performance for the hydrogenation of HMF was evaluated in a 100 mL steel autoclave equipped with a mechanical stirrer. HMF (4.0 mmol) with toluene (0.25 mL) as an internal standard was initially dissolved in *n*-butanol (20 mL) in the reactor, and then the fresh reduced catalyst (0.050 g) was added. The autoclave was purged thrice with H_2 and heated up to the desired temperature. Afterward, the reactor was cooled to RT and decompressed. The gas phase products were detected with a gas chromatograph (with H_2 as a carrier gas) equipped with a Porapak Q column (3 m × 3 mm) and a thermal conductivity detector. The liquid phase products were detected with a gas chromatograph equipped with a flame ionization detector and an HP-5 capillary column (30 m × 0.32 mm × 0.25 μm) to quantify HMF, FDM, MFM, DMF, and DMTHF. The standard samples such as HMF, DMF, MFM, FDM, DMTHF, and MF were purchased from J&K Scientific Ltd. The ether compounds formed in the reaction were qualitative by a gas chromatography-mass spectrometer (GC–MS) equipped with an HP-5 capillary column. The typical GC chart is shown in Figure S4. Toluene was added to calculate the correction factors for products and monitor the carbon balance. The correction factor for all unknown compounds was set to 1. The calibrated area of each compound was normalized to calculate the conversion and product selectivities. In the recycling process, the catalyst was initially separated with a magnet and then washed several times with *n*-butanol. The catalyst was ready for another recycle after drying at 373 K according to the previous procedures.

Acknowledgements

We acknowledge the financial support from the Ministry of Science and Technology of China (grant no. 2011CBA00508), the Natural Science Foundation of China (grant nos. 21173175, 21303141, 21403178, and 21473145), the Research Fund for the Doctoral Program of Higher Education (grant no. 20110121130002), the Postgraduate Basic Innovative Research Program of Xiamen University (program no. 201412G001), and the Program for Innovative Research Team in Chinese Universities (program no. IRT 14R31).

Keywords: bimetallic catalysts · 2,5-dimethylfuran · hydrogenation · 5-hydroxymethylfurfural · nanoparticles

[1] a) P. Gallezot, *Chem. Soc. Rev.* **2012**, *41*, 1538–1558; b) K. Barta, P. C. Ford, *Acc. Chem. Res.* **2014**, *47*, 1503–1512.
[2] J. J. Bozell, G. R. Petersen, *Green Chem.* **2010**, *12*, 539–554.
[3] a) O. Casanova, S. Iborra, A. Corma, *ChemSusChem* **2009**, *2*, 1138–1144; b) S. E. Davis, B. N. Zope, R. J. Davis, *Green Chem.* **2012**, *14*, 143–147; c) H. Ait Rass, N. Essayem, M. Besson, *Green Chem.* **2013**, *15*, 2240–2251; d) A. Villa, M. Schiavoni, S. Campisi, G. M. Veith, L. Prati, *ChemSusChem* **2013**, *6*, 609–612.
[4] a) M. Tamura, K. Tokonami, Y. Nakagawa, K. Tomishige, *Chem. Commun.* **2013**, *49*, 7034–7036; b) S. Subbiah, S. P. Simeonov, J. M. S. S. Esperanca, L. P. N. Rebelo, C. A. M. Afonso, *Green Chem.* **2013**, *15*, 2849–2853; c) Y. Kwon, E. de Jong, S. Raoufmoghaddam, M. T. Koper, *ChemSusChem* **2013**, *6*, 1659–1667.
[5] L. Hu, L. Lin, S. J. Liu, *Ind. Eng. Chem. Res.* **2014**, *53*, 9969–9978.
[6] Y. H. Zu, P. P. Yang, J. J. Wang, X. H. Liu, J. W. Ren, G. Z. Lu, Y. Q. Wang, *Appl. Catal. B* **2014**, *146*, 244–248.
[7] T. Thananatthanachon, T. B. Rauchfuss, *Angew. Chem. Int. Ed.* **2010**, *49*, 6616–6618; *Angew. Chem.* **2010**, *122*, 6766–6768.
[8] a) T. S. Hansen, K. Barta, P. T. Anastas, P. C. Ford, A. Riisager, *Green Chem.* **2012**, *14*, 2457–2461; b) D. Scholz, C. Aellig, I. Hermans, *ChemSusChem* **2014**, *7*, 268–275.
[9] P. Nilges, U. Schröder, *Energy Environ. Sci.* **2013**, *6*, 2925–2931.
[10] a) J. H. Zhang, L. Lin, S. J. Liu, *Energy Fuels* **2012**, *26*, 4560–4567; b) L. Hu, X. Tang, J. X. Xu, Z. Wu, L. Lin, S. J. Liu, *Ind. Eng. Chem. Res.* **2014**, *53*, 3056–3064.
[11] M. Chatterjee, T. Ishizaka, H. Kawanami, *Green Chem.* **2014**, *16*, 1543–1551.
[12] J. Mitra, X. Y. Zhou, T. Rauchfuss, *Green Chem.* **2015**, *17*, 307–313.
[13] Y. Román-Leshkov, C. J. Barrett, Z. Y. Liu, J. A. Dumesic, *Nature* **2007**, *447*, 982–986.
[14] S. Nishimura, N. Ikeda, K. Ebitani, *Catal. Today* **2014**, *232*, 89–98.
[15] G. H. Wang, J. Hilgert, F. H. Richter, F. Wang, H. J. Bongard, B. Spliethoff, C. Weidenthaler, F. Schüth, *Nat. Mater.* **2014**, *13*, 293–300.
[16] X. Kong, Y. F. Zhu, H. Y. Zheng, F. Dong, Y. L. Zhu, Y. W. Li, *RSC Adv.* **2014**, *4*, 60467–60472.
[17] Y. B. Huang, M. Y. Chen, L. Yan, Q. X. Guo, Y. Fu, *ChemSusChem* **2014**, *7*, 1068–1070.
[18] A. J. Kumalaputri, G. Bottari, P. M. Erne, H. J. Heeres, K. Barta, *ChemSusChem* **2014**, *7*, 2266–2275.
[19] R. M. M. Abbaslou, A. Tavassoli, J. Soltan, A. K. Dalai, *Appl. Catal. A* **2009**, *367*, 47–52.
[20] Z. Y. Hou, O. Yokota, T. Tanaka, T. Yashima, *Appl. Catal. A* **2003**, *253*, 381–387.
[21] a) B. D. Li, J. Wang, Y. Z. Yuan, H. Ariga, S. Takakusagi, K. Asakura, *ACS Catal.* **2011**, *1*, 1521–1528; b) W. J. Li, L. M. Ye, P. Long, J. Chen, H. Ariga, K. Asakura, Y. Z. Yuan, *RSC Adv.* **2014**, *4*, 29072–29082.
[22] S. Sitthisa, W. An, D. E. Resasco, *J. Catal.* **2011**, *284*, 90–101.
[23] a) P. Panagiotopoulou, N. Martin, D. G. Vlachos, *J. Mol. Catal. A* **2014**, *392*, 223–228; b) M. Balakrishnan, E. R. Sacia, A. T. Bell, *Green Chem.* **2012**, *14*, 1626–1634.
[24] J. Luo, L. Arroyo-Ramírez, R. J. Gorte, D. Tzoulaki, D. G. Vlachos, *AIChE J.* **2015**, *61*, 590–597.
[25] L. M. Ye, X. P. Duan, H. Q. Lin, Y. Z. Yuan, *Catal. Today* **2012**, *183*, 65–71.

Received: February 1, 2015
Revised: March 23, 2015
Published online on ■■ ▮▮, 0000

*L. Yu, L. He, J. Chen, J. Zheng, L. Ye,**
*H. Lin, Y. Yuan**

■■ – ■■

Robust and Recyclable Nonprecious Bimetallic Nanoparticles on Carbon Nanotubes for the Hydrogenation and Hydrogenolysis of 5-Hydroxymethylfurfural

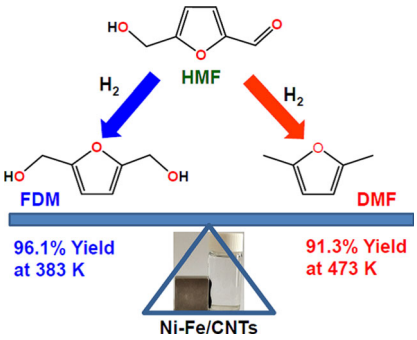

Benefits of selective memory: The alloying effect of nonprecious Ni–Fe on carbon nanotubes is beneficial to the selective hydrogenation and hydrogenolysis of 5-hydroxymethylfurfural, which gives high selectivities to 2,5-furandimethanol or 2,5-dimethylfuran depending on the reaction temperature. The catalyst can be easily separated with a magnet and reused several times without significant loss of activity.